


## Electric energy dissipation and electric tortuosity in electron conductive cement-based materials

Nancy A. Soliman <sup>1</sup>, Nicolas Chanut,<sup>2</sup> Vincent Deman,<sup>2</sup> Zoe Lallas,<sup>1</sup> and Franz-Josef Ulm <sup>1,2,\*</sup>

<sup>1</sup>*Department of Civil and Environmental Engineering, Massachusetts Institute of Technology, Cambridge, Massachusetts 02139, USA*

<sup>2</sup>*Joint MIT-CNRS Unit Materials Science for Energy and Environment, MIT Energy Initiative, Cambridge, Massachusetts 02139, USA*

 (Received 14 July 2020; revised 17 October 2020; accepted 17 November 2020; published 9 December 2020)

The emergence of multifunctional cement-based materials in the construction industry has the potential to shift the paradigm from strength-only performance to new functionalities enabled by electron conducting capabilities in one of the most material- and energy-intensive industry sectors worldwide. To enable such developments, we present results of a hybrid experimental-theoretical investigation of the electrical conductivity and resistive (Joule) heating of highly heterogeneous nanocarbon (nCB)-cement-based composites (pastes and mortars). By analogy with diffusivity, we find that electrical conductivity is determined by the electric tortuosity of a “volumetric wiring” permeating a highly heterogeneous matrix from percolation to saturation. From a combination of electrical conductivity and Joule heat rate measurements, we show that the electric energy dissipation at the origin of the Joule heating originates from spatial electric-field fluctuations, reminiscent of the fluctuation-dissipation theorem. We report that these fluctuations—in first order—are well captured by functional relations of the electric tortuosity of the composite material, and synthesize these observations into a first-order dissipation-tortuosity model. We suggest that harvesting the benefits of electron conducting cement-based materials, such as resistive heating, electromagnetic shielding, and energy storage, will ultimately focus on settling the competition between conductor concentration and electric tortuosity. Given the global environmental footprint of concrete, the results open venues for the sustainable development of concrete for existing and emerging green technology applications.

DOI: [10.1103/PhysRevMaterials.4.125401](https://doi.org/10.1103/PhysRevMaterials.4.125401)

### I. INTRODUCTION

The introduction of electron conducting bulk composites in the construction industry [1–7], in which highly electron conductive constituents (such as graphite powder, carbon black, carbon nanotubes, as well as steel and carbon fibers) are mixed with insulating construction materials in bulk (cement paste, mortar, concrete), is based upon the dual premise that (i) engineers will be able to harvest the many benefits that result from electron conductivity [4] and (ii) these benefits will outweigh the significant environmental footprint of construction materials, specifically concrete [8]. These benefits range from the ability to generate heat through current flowing through a conductor, known as resistive heating or Joule effect, e.g., for radiant heating of slabs [5], walls, and pavements [6,9,10], to electromagnetic shielding [2,4,11] and the storage of electric energy by using these materials as electrodes in structural capacitor elements in electrical energy storage (EES) systems [7,12] (see the Supplemental Material (SM-I) [13]).

Since the early developments of bulk metal and carbon-based conductive polymer composites, it has been well known that the electron conduction capacity of conductor-insulator composites relies on the development of a percolated electron conductive network through an insulator [14]. While the physics of the phenomenon, specifically around the percolation threshold, has been intensively studied [15–19],

the governing mechanisms that link measurable electric properties to constituent and texture properties of highly heterogeneous conductor-insulator composites, as visible in scanning electron microscope (SEM) images [Figs. 1(e) and 1(f)], still remain to be revealed.

Here, we focus on the assessment of electrical conductivity and Joule heating in nanocarbon-black (nCB) loaded cement-based materials (pastes, mortars), and approach the problem by means of a hybrid experimental-modeling approach in which we blend experimental observations with concepts of composite mechanics adapted, by analogy, for electric charge flow through heterogeneous materials.

Our typical experimental setup for Joule heating measurements is shown in Fig. 1(a): a cylindrical sample (cross section  $A = \pi r_0^2$ , length  $L$ ) tightly clamped in between two conducting plates [here, graphite foil, a current collector with a conductivity higher than the material to be tested and mounted insulated to drive the current into the sample and not in other elements of the system; see Fig. 1(a)]. In the first set of experiments, an electric potential difference is applied using a DC generator (Potentiostat Solartron SI1287). The current  $I$  is measured and the resistance is determined from Ohm’s law,  $R = U_0/I$ . The measurements are carried out with a voltage ramp  $U_0 = 0\text{--}10$  V of rate 100 mV/s, which entails an on-average negligible temperature increase over the ramp time of 100 s (see SM-II B [13]). The sample resistance fit to the recorded  $U_0 - I$  curve during the ramp provides a means to determine the sample’s electrical conductivity,  $\sigma_{\text{exp}} = L/(RA)$  (of unit S/m). Moreover, to quantify the magnitude of the

\*Corresponding author: [ulm@mit.edu](mailto:ulm@mit.edu)

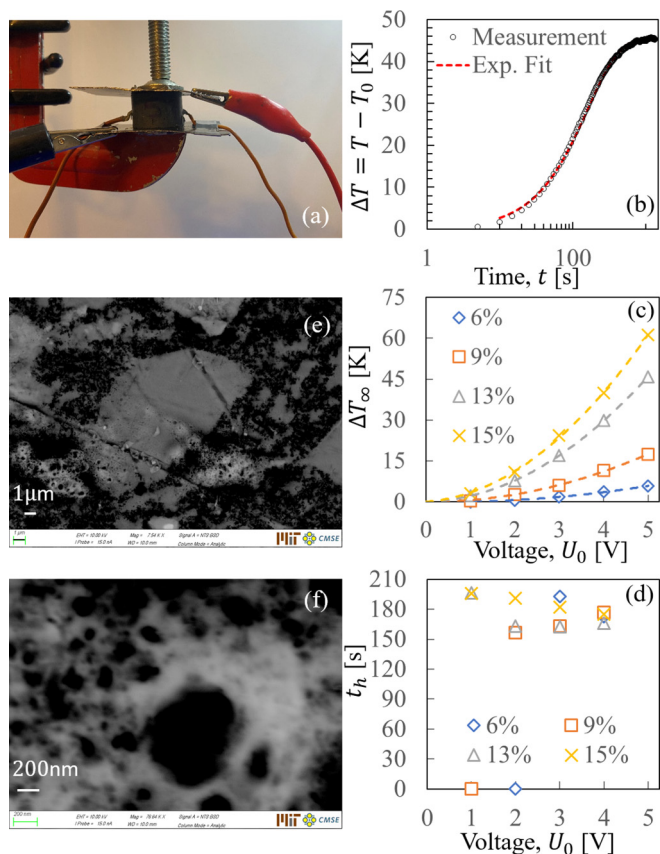


FIG. 1. (a) Experimental setup: a sample clamped between two conductive graphite foils connected to a voltage generator, with two thermocouples placed in the center. (b) Measured and fitted temperature rise,  $\Delta T(t) = T(t) - T_0$ . (c) Asymptotic temperature rise  $\Delta T_\infty$  and (d) characteristic time  $t_h$  as a function of the applied electric potential difference  $U_0$  for different carbon-black volume fractions  $\varphi$  of a W/C = 0.42 cement paste. (e), (f) SEM images of a porous carbon-black particle network (black) in a highly heterogeneous cement paste matrix (W/C = 0.42,  $\varphi = 13\%$ ).

resistive (Joule) heating of the composite, a second experiment is carried out, with the same equipment, at constant applied voltage  $U_0$  (1–5 V), while simultaneously measuring the temperature increase in time,  $T(t) = T_0 + \Delta T(t)$ , with respect to room temperature ( $T_0$ ), by means of type K thermocouples placed at half length of the cylindrical specimen into predrilled holes (diameter 1 mm), which are sealed after placement with a thermal paste to ensure good thermal conductivity between the sample and the thermocouple [Fig. 1(a)], and connected to a Fluke 287 True-RMS Stand Alone Logging Multimeter. For each constant voltage level, the temperature development exhibits an exponential time evolution,  $\Delta T(t) = \Delta T_\infty(1 - e^{-t/t_h})$ , to a maximum temperature [Fig. 1(b)] as a consequence of the Joule effect, as well known from other electron conductive bulk composites (for instance, carbon-black loaded rubbers [20,21]; see, also, SM-II A [13]). In such experiments, the maximum temperature rise,  $\Delta T_\infty = T(\infty) - T_0$ , is found to scale with the square of the applied voltage,  $\Delta T_\infty \sim U_0^2$  [Fig. 1(c)], consistent with Joule’s law. Furthermore, as one would expect, the maximum temperature increases with the nCB concentration [Fig. 1(c)],

whereas the characteristic time of heating is not affected by the nCB volume fraction [Fig. 1(d)]. While both measurable quantities,  $\Delta T_\infty = \bar{\mu}_{\text{exp}} V / (Sh)$  and  $t_h = V(\rho_m C_m) / (Sh)$ , depend on sample volume  $V$  and surface  $S = 2\pi r_0 L$ , through which heat escapes (heat exchange coefficient  $h$ ; see SM-II [13]), a straightforward solution of the governing heat equation provides a means to determine the intrinsic Joule heating rate from  $\bar{\mu}_{\text{exp}} = (\Delta T_\infty / t_h) \rho_m C_m$ , where an overbar stands for volume averaging and  $\Delta T_\infty / t_h$  is the initial slope of the experimentally accessible exponential temperature-time curve [Fig. 1(b)]; whereas  $\rho_m C_m$ ,  $\rho_m$ , and  $C_m$  stand for, respectively, the sample’s volume heat capacity, mass density, and specific heat capacity of the constituents of the conductor-insulator composite material; here, nanocarbon-black particles, unhydrated cement, hydration products, and sand are included.

## II. RESULTS

We start by measuring the electron conductivity and resistive heating of a comprehensive set of 43 electron conducting nCB–cement-based composites that vary strongly in composition of the conducting phase (a nanocarbon-black additive, PBX55, of a BET (Brunauer-Emmett-Teller) nitrogen surface area of 45–60  $\text{m}^2/\text{g}$ , and density of 1.7–1.9  $\text{g}/\text{cc}$  [22]), pore space, and insulating phases (cement paste and sand). This was achieved by varying the mix proportions, namely, the water-to-cement (W/C) mass ratio, and the addition of sand at different sand-to-paste mass ratios (mortar 1:1 and mortar 2:1), while fine tuning the nCB concentration for maximum electrical conductivity (see SM-III [13]) through the use of surfactants [here, polynaphthalene sulfonate (PNS) and superplasticizer-based high-range water-reducing admixture (HRWRA)]. (For sample preparation, see SM-III [13]).

### A. Electrical conductivity

Figure 2(a) displays the measured electrical conductivity ( $\sigma_{\text{exp}}$ ) vs carbon-black volume fraction ( $\varphi \pm \Delta\varphi$ ) determined from density measurements of the hardened samples (see SM-III C [13]). Similar to other electron conducting bulk materials [14], we find that carbon-black loaded cement pastes and mortars become electron conducting beyond a very low and clearly defined percolation threshold [inset of Fig. 2(a)],  $\varphi_c = 0.039$  [with 95% confidence bounds (0.020, 0.058)]. Beyond the percolation threshold, the electrical conductivity ( $\sigma_{\text{exp}}$ ) scales with the carbon volume fraction  $\varphi$ , as  $\sigma_{\text{exp}} \sim (\varphi - \varphi_c)^{\alpha_c}$  ( $R^2 = 0.9485$ ) [inset of Fig. 2(a)], with a conductivity exponent  $\alpha_c = 1.35$  [with 95% confidence bounds (0.97, 1.73)], in accordance with conduction-percolation relations derived by Kirkpatrick [15] and Stauffer [23].

### B. Joule heating

The second series of measurements that we explore is the resistive heating rate. We take into account the experimental evidence of Joule’s law [Fig. 1(c)] and normalize the experimentally accessible volumetric heat rate  $\bar{\mu}_{\text{exp}}$  by the square of the applied electric field,  $E_0^2 = (U_0/L)^2$ , corrected for the

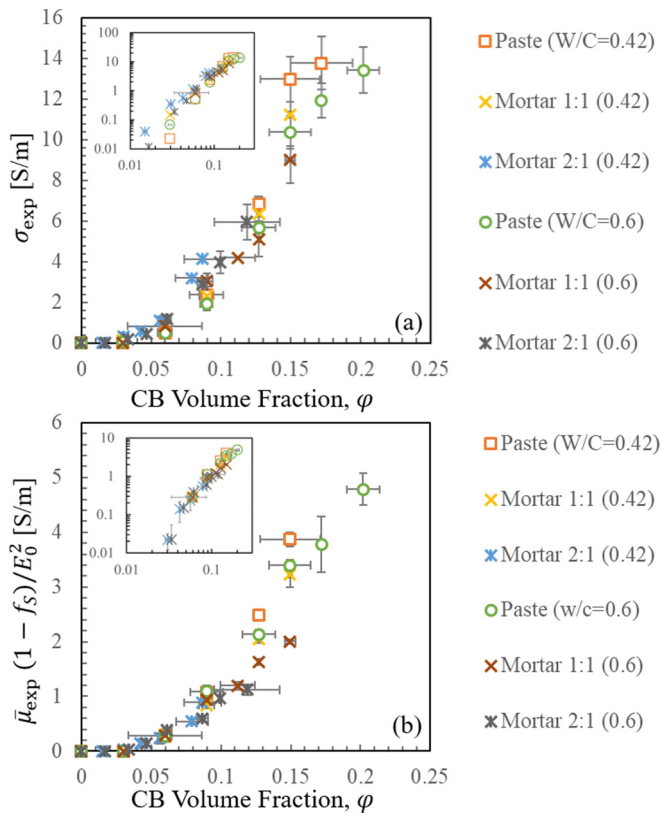


FIG. 2. Measured electrical conductivity ( $\sigma_{\text{exp}}$ ) and resistive heating/Joule effect ( $\bar{\mu}_{\text{exp}}$ ) vs carbon-black volume fraction  $\varphi$ . (a) Electrical conductivity  $\sigma_{\text{exp}}$  determined from electric resistance measurements. (b) Resistive heating (Joule effect) determined from the measured temperature rise in time due to the application of a potential difference (voltage  $U_0 = E_0 L$ , with  $L$  sample length), corrected for the (insulating) sand volume fraction  $f_s$ . [Horizontal error bars  $\Delta\varphi$  represent the relative error in mass density fit (see SM-III [13]); vertical error bars represent the standard deviation of five heating tests carried out at different voltages,  $U_0 = 1\text{--}5$  V (see the table of all the results in the SM [13])]. The insets display plots in a log-log scale, showing an almost identical percolation threshold,  $\varphi_c = 3\text{--}4\%$ , for both electrical conductivity and Joule effect, yet a different exponent in the scaling  $(\varphi - \varphi_c)^{\alpha_i}$ , with a fitted conductivity exponent  $\alpha_C = 1.35$  and fitted Joule effect exponent  $\alpha_J = 1.57$ .

presence of the insulating sand inclusion phase,

$$\frac{\bar{\mu}_{\text{exp}}}{E_0^2(1 - f_s)} = \frac{\Delta T_{\infty}}{t_h} \frac{\overline{\rho_m C_m}}{E_0^2} (1 - f_s). \quad (1)$$

The sample's heat capacity,  $\overline{\rho_m C_m} = \sum_{i=(CB,P,S)} f_i \rho_i C_i$ , is determined from volume fractions ( $f_i$ ) of carbon black (CB,  $f_{CB} = \varphi$ ), cement paste (P), and sand inclusions (S), together with characteristic values of the specific heat capacity of the constituents:  $C_{CB} = 710\text{--}800$  J/(kg K) for carbon black,  $C_P = 920$  J/(kg K) for cement paste [24], and  $C_S = 830$  J/(kg K) for sand. The obtained results are displayed in Fig. 2(b). Not surprisingly, the resistive heating exhibits an (almost) identical percolation threshold as electrical conductivity [inset of Fig. 2(b)],  $\varphi_c = 0.033$  [with 95% confidence bounds (0.008, 0.057)], and follows a power relationship,  $\bar{\mu}_{\text{exp}} \sim (\varphi - \varphi_c)^{\alpha_J}$  ( $R^2 = 0.9485$ ), but with an exponent  $\alpha_J = 1.57$

[with 95% confidence bounds (1.10, 2.04)] that differs from the conductivity exponent by 15%. This suggests that the electrical conductivity and resistive heating may not be proportional. That is, while both electrical conductivity and Joule heating relate to electron flow [as exemplified by the (almost) identical percolation threshold], the experimental results provide evidence of a difference in the underlying mechanisms and properties that define the development of the two phenomena in such highly disordered conductor-insulator composites.

### III. DISCUSSION

We proceed by developing a first-order quantitative framework to explain the experimental observations using tools of composite mechanics (see, e.g., [25,26]). We adopt this approach, by analogy, for assessing the link between electron flow, constituent behavior, texture, and macroscopically measurable electrical conductivity and Joule heating rate.

#### A. Experimental electric tortuosity assessment

Following the test setup, we consider the conductor-insulator composite sample subject to a regular electric field at the boundary,  $\partial V$ , such that

$$\text{on } \vec{z} \in \partial V; u = \vec{E} \cdot \vec{z}; \vec{E} = \overline{\vec{e}(\vec{z})}, \quad (2)$$

where  $u$  is the electric potential difference, and  $\vec{e}(\vec{z})$  and  $\vec{E} = E_0 \vec{n}_z$  stand, respectively, for the microscopic (position vector  $\vec{z}$ ) and the macroscopic electric field ( $E_0 = U_0/L$  for a voltage applied on the cylinder end sides in the direction of the cylinder axis  $\vec{n}_z$ ). The voltage boundary condition (2) is the electric potential difference representative of the work needed to bring charge from one side of the sample to the other in an electric field. Under steady-state conditions, the local electric field is given by Maxwell's (first) equation,  $\nabla \cdot \vec{e} = \rho_0/\varepsilon_0$ , with  $\rho_0$  the volumetric charge density and  $\varepsilon_0$  the permittivity. The electric field determines the current density, both locally,  $\vec{j}(\vec{z}) = \sigma(\vec{z}) \vec{e}(\vec{z})$ , and globally,  $\vec{J} = \sigma_{\text{hom}} \vec{E}$ . This means that volume averaging provides a link between the spatially varying local electrical conductivity  $\sigma(\vec{z})$  and the composite electrical conductivity  $\sigma_{\text{hom}}$ . For an isotropic two-phase material composed of a conducting phase [volume fraction  $\varphi$ ; conductivity  $\sigma(\vec{z}) = \sigma_0$ ] and an insulator [volume fraction  $1 - \varphi$ ;  $\sigma(\vec{z}) = 0$ ], we obtain

$$\vec{J} = \overline{\vec{j}(\vec{z})}; \frac{\sigma_{\text{hom}}}{\sigma_0} = \varphi \frac{\overline{\vec{e}(\vec{z})^{V_c} \cdot \vec{n}_z}}{E_0}, \quad (3)$$

where  $\overline{\vec{e}(\vec{z})^{V_c}}$  stands for the volume average of the local electrical field taken over the volume of the conducting phase,  $V_c = \varphi V$ .

An interesting analogy can be made here between the electron conductivity of a conductor-insulator composite and the diffusive mass flux of a solute through a solvent in a porous material [26,27]. More specifically, in contrast to approaches in soil science, which employ an ion-conductivity analogy to estimate the hydraulic conductivity of porous materials [28,29], we consider the local electric potential difference [voltage  $u(\vec{z})$ ] in the connected electron conducting phase of volume fraction  $\varphi = V_c/V$  as an analog of the main diffusion



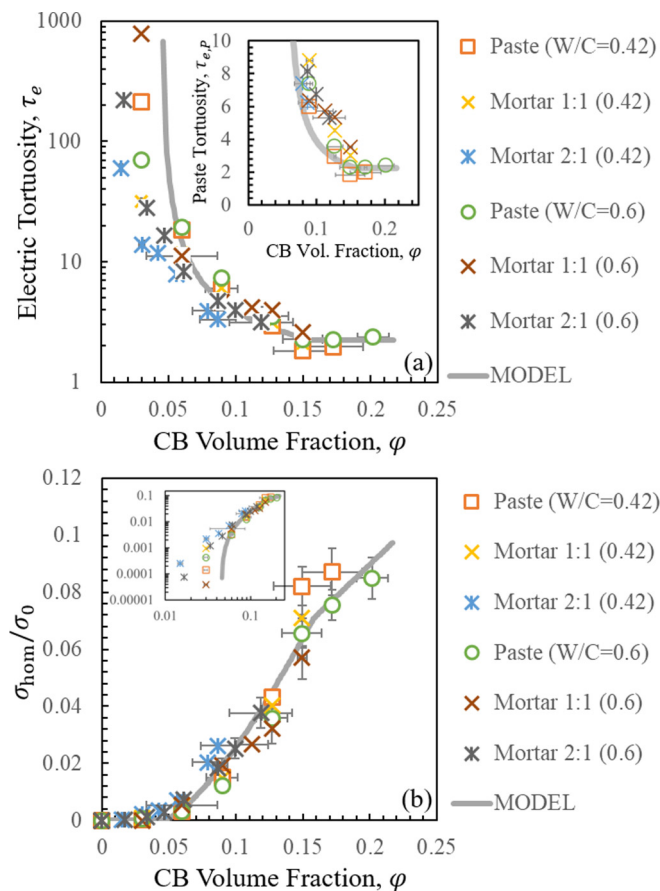


FIG. 3. Electric tortuosity assessment and modeling. (a) Electric tortuosity ( $\tau_e$ ) vs carbon-black volume fraction ( $\phi$ ). Inset: paste electric tortuosity  $\tau_{e,P} = \tau_e/(1 - f_s)$  (with  $f_s$  the sand volume fraction). (b) Tortuosity-based model performance: normalized electrical conductivity ( $\sigma/\sigma_0$ ). Inset: model performance in a log-log scale. [Model parameters: base electrical conductivity  $\sigma_0 = 158$  S/m; percolation threshold  $\phi_c = 4.5\%$ ; saturation concentration  $\phi_0 = 15.8\%$ ; minimum electric tortuosity of  $\tau_e(\phi_0) = 2.23$ ].

variable, solute mass density  $\rho(\vec{z})$ , in a solvent saturating the connected porosity. The analog of Fick's diffusive flux,  $\vec{j} = -D\nabla\rho$ , is the current intensity,  $\vec{j} = \sigma\nabla u$ , with  $\vec{e} = \nabla u$ . Finally, the analog of mass conservation,  $\nabla \cdot \vec{j} = 0$ , is Maxwell's equation,  $\nabla \cdot (\vec{e} - \vec{e}_0) = 0$  with  $\vec{e}_0 = \rho_0/\epsilon_0 \vec{z}$ . This diffusion-conductivity analogy permits a quantification of the electric tortuosity effects,

$$\frac{\sigma_{\text{hom}}}{\sigma_0} = \frac{\phi}{\tau_e}; \quad \tau_e = \frac{E_0}{\vec{e} \cdot \vec{n}_z V_c}. \quad (4)$$

Much akin to classical definitions of tortuosity (see, e.g., [29]), the electric tortuosity  $\tau_e$ , herein defined, can be viewed—in first order—as a *geometric* tortuosity, that is, the mean path ( $\ell$ ) taken by electrons crossing the samples, normalized by sample length ( $L$ ); i.e.,  $\tau_e \simeq \ell/L$ . It should be noted that other phenomena, such as electron tunneling effects [18]—no doubt—equally affect the flow path of electrons, specifically around the percolation threshold.

The relevance of the tortuosity analogy is depicted in Fig. 3(a) in the form of a plot of the experimental accessible

electric tortuosity  $\tau_e \sim \phi/\sigma_{\text{exp}}$  vs the carbon content  $\phi$ . The inset of Fig. 3(a) corrects this experimental tortuosity for the insulating sand phase by considering the carbon-black–paste tortuosity,  $\tau_{e,P} = \tau_e/(1 - f_s)$ . For both the composite and the paste, the tortuosity is found to collapse onto a master curve for all carbon-black–cement paste and mortar composite materials. It decreases with increasing (overall) carbon content  $\phi$  from the percolation threshold, where  $\tau_e \rightarrow \infty$  (unconnected carbon-black grains), to a horizontal asymptote, where the carbon-black–paste composite realizes a minimum electric tortuosity,  $\tau_e(\phi > \phi_0) = \tau_e(\phi_0)$ . The asymptotic behavior of electric tortuosity around the percolation threshold is reminiscent of results obtained by both molecular dynamics simulations of a conductive gel formation, due to interparticle electron tunneling phenomena [18], and experimental assessment of percolation phenomena in carbon-black suspensions [19]. This suggests that the phenomena enabling the very low percolation threshold [ $\phi_c \simeq 3\text{--}4\%$ , inset of Fig. 2(a)] is independent of the specific mix design parameters of the electron conducting bulk composite, and relate to the very nature of the carbon-black gelation process. On the other hand, the asymptotic minimum electric tortuosity of the electron conducting bulk composite,  $\tau_e(\phi_0)$ , is attributed to the texture of the conductive network of carbon black.

To quantitatively capture these observations, we consider the connected network of carbon black as a “volumetric wiring” which permeates the system from percolation to saturation. The volumetric wire originates (most likely) during the early stages of gelation from a phase separation process of the hydrophobic carbon black and the hydrophilic cement, water, sand, and so on. That is, the volumetric wire is not a homogeneous phase, but a composite of CB particles (of packing density  $\eta_{CB} = 0.60\text{--}0.67$ ; see SM-III C [13]) and cement hydration products, as evidenced by mass density measurements (SM-III C [13]) and visible in SEM images [Figs. 1(e) and 1(f)]. Consistent with percolation theory, the percolation threshold of the volumetric wire phase is well above the carbon-black volume fraction percolation threshold of  $\phi_c \sim 3\text{--}4\%$  determined from conductance measurements [inset of Fig. 2(a)]. In fact, it should be close to the site percolation threshold of a simple cubic lattice,  $p_c = 0.3115 \pm 0.0005$  [30], as known from percolation studies of a conductive phase in a bulk insulator [15], or, in the continuum limit of a disordered system, to the percolation threshold of the self-consistent diffusion model,  $p_c = 1/3$  [27], when written—by analogy—for electrical conductivity and electric tortuosity,

$$\frac{\sigma_{\text{hom}}}{\sigma_0} = \frac{(\phi - p_c)}{1 - p_c} \geq 0; \quad \tau_e = \frac{1 - p_c}{\phi - p_c} \phi. \quad (5)$$

Herein,  $\sigma_0$  is a reference electrical conductivity and  $\phi$  is the volume fraction of the volumetric wire in the composite (to be distinguished from the CB volume fraction  $\phi$  in the composite). We need to adapt percolation theory and self-consistent modeling to the experimental evidence [Fig. 3(a)] and bridge between the two tortuosity asymptotes: a vertical one at the percolation threshold,  $\phi^+ \rightarrow p_c$  where  $\tau_e \rightarrow \infty$ , and a horizontal one for  $\phi \rightarrow 1$  ( $\phi \rightarrow \phi_0$ ), where the volumetric wire saturates the composite system at a minimum tortuosity of  $\tau_e \rightarrow \tau_e(\phi_0)$ . This is achieved here by considering the differential homogenization approach [27,31]. Starting from the

system with minimum tortuosity  $\tau_e(\varphi_0)$ , we infinitesimally remove the conducting phase,  $-d\phi > 0$ , by adding an insulator (paste, sand, etc.). After each increment, the electrical conductivity is evaluated. The first step is given by Eq. (5); the  $k$ th step consists in removing an infinitesimal fraction  $d\epsilon \ll 1$  of the homogenized medium in excess of the percolation threshold, and in replacing it by the same volume of insulator,  $(\phi - p_c)d\epsilon = -d\phi$ . In this step, we apply the self-consistent solution (5) for the introduction of  $d\epsilon$ , while considering  $\sigma = \varphi/\tau_e$  and  $d\sigma = d\varphi/\tau_e - \varphi d\tau_e/\tau_e^2$ . Finally, we integrate from the reference state [the minimum tortuosity,  $\tau_e(\varphi_0)$ ] to any value  $p_c < \phi < 1$  above the percolation threshold  $p_c$  to obtain the electrical conductivity relative to the reference electrical conductivity,  $\sigma_{\text{hom}}(\varphi_0)/\sigma_0 = \varphi_0/\tau_e(\varphi_0)$ , while letting  $\phi(\varphi) = \varphi/\varphi_0 \leq 1$  and  $\phi(\varphi) - p_c = (\varphi - \varphi_c)/\varphi_0$  (see SM-IV [13]):

$$0 \leq \frac{\sigma_{\text{hom}}}{\sigma_0} = \frac{\varphi_0}{\tau_e(\varphi_0)} \left( \frac{\varphi - \varphi_c}{\varphi_0 - \varphi_c} \right)^{\frac{\varphi_0}{\varphi_0 - \varphi_c}} \leq \frac{\varphi}{\tau_e(\varphi_0)}. \quad (6)$$

This first-order electrical conductivity model is similar to the conduction-percolation relations derived by Kirkpatrick [15] and Stauffer [23], which are of the form  $\sigma_{\text{hom}} \sim \sigma_0(p - p_c)^{\alpha_c}$ , with  $p$  the probability of finding the conducting phase that is equivalent to the volume fraction of the conducting phase above the critical concentration, and  $p_c$  is the critical or threshold probability of formation of a conducting network; whereas  $\alpha_c$  is the conductivity exponent. The added value of the differential model herein employed is that it explicitly links the probabilities and exponent to measurable volume fractions, namely,  $p = \varphi/\varphi_0$ ,  $p_c = \varphi_c/\varphi_0$ , and  $\alpha_c = \varphi_0/(\varphi_0 - \varphi_c)$ . The specific behavior for  $\varphi > \varphi_0$  as predicted by Eq. (6) is motivated by the evidence of a minimum tortuosity,  $\tau_e(\varphi_0)$ , associated with the volumetric wires saturating the sample bulk, beyond which the electrical conductivity is expected to increase linearly with the carbon-black concentration, quasi-uniformly enhancing the carbon content of the volumetric wires.

In Fig. 3, we display the model performance in terms of the electric tortuosity  $\tau_e(\varphi) = \varphi/(\sigma_{\text{hom}}/\sigma_0)$  [Fig. 3(a)] and the normalized electrical conductivity  $\sigma_{\text{hom}}/\sigma_0$  [Fig. 3(b)]. The model has four adjustable parameters, which are readily obtained by minimizing the quadratic error between the electrical conductivity measurements (of 43 samples) and model predictions ( $R^2 = 0.9614$ ): (i) a reference electrical conductivity  $\sigma_0 = 158$  S/m [with 95% confidence bounds (60, 256) S/m], in good agreement with experimental values reported from conductivity measurements of highly compacted carbon-black powder [32]; (ii) a carbon-black percolation threshold  $\varphi_c = \varphi_0 p_c = 4.5\%$  [with 95% confidence bounds (2.3, 6.7)%], which is slightly above the experimentally observed percolation threshold [inset of Fig. 3(b)] and which permits estimating a site percolation threshold,  $p_c = 29\%$ , close to the simple cubic lattice percolation threshold of 31% [30]; (iii) a saturation concentration  $\varphi_0 = 15.8\%$  [with 95% confidence bounds (11.4, 20.2)%] (at which the composite material reaches its minimum electric tortuosity); and (iv) the corresponding minimum electric tortuosity  $\tau_e(\varphi_0) = 2.23$  [with 95% confidence bounds (1.60, 2.85)].

## B. Fluctuation-based assessment of Joule heating

We proceed in a similar fashion with an analysis of the resistive heating rate by making use of concepts of nonlinear homogenization techniques employed for a variety of material properties ranging from strength properties [25,26] to viscosity and yield stress of slurries [33]. Our starting point is Joule's (first) law at a microscale,  $\mu(\vec{z}) = \vec{j}(\vec{z}) \cdot \vec{e}(\vec{z})$ . The volume averaging then provides

$$\mu_{\text{hom}} = \overline{\mu(\vec{z})} = \varphi \sigma_0 \overline{\vec{e}(\vec{z}) \cdot \vec{e}(\vec{z})}^{V_c}. \quad (7)$$

In contrast to the electrical conductivity upscaling relation (3), which only involves a linear average of the electric field, the resistive heating is governed by the quadratic average of the electric field, and thus by spatial fluctuations of the microscopic electric field. Further insight is provided by a development of the extended Hill Lemma (e.g., [34]) for Maxwell's equation (see SM-V [13]),

$$\mu_{\text{hom}} = \vec{J} \cdot \vec{E} - \varphi \sigma_0 \overline{\frac{\rho_0}{\epsilon_0}(\vec{z}) u(\vec{z})}^{V_c}, \quad (8)$$

where  $u(\vec{z})$  is the local potential difference in the electron conducting phase. The first term,  $\vec{J} \cdot \vec{E} = \sigma_{\text{hom}} E_0^2$ , represents the work rate of the macroscopic charge flow (macroscopic current density  $\vec{J}$ ) in the applied (macroscopic) electric field,  $\vec{E} = E_0 \vec{n}_z$ , whereas the second term,  $\varphi \sigma_0 \overline{(\rho_0/\epsilon_0) u}^{V_c}$ , can be viewed as the work rate of the local charge density of the conductor phase (volume  $V_c$ ) due to a local potential difference  $u(\vec{z})$  in the heterogeneous microstructure. For a "perfect" conductor, the two terms would cancel each other out, resulting in a zero resistive heating. In contrast, the difference between the two terms is the power dissipated in the conductor, which leads to Joule heating due to texture imperfections of the volumetric wiring. That is, reminiscent of the fluctuation-dissipation theorem, Eqs. (7) and (8) link, at the composite scale, Joule heating to electric-field fluctuations and electric-field dissipation.

Furthermore, to assess the dissipation due to fluctuations explicitly from measurements, it is useful to normalize the Joule heating rate by a reference heat sink term, representative of the work rate of the reference conductor (electrical conductivity  $\sigma_0$ ), when a constant potential difference is applied, i.e.,  $\mu_0 = \sigma_0 \overline{\vec{e} \cdot \vec{e}}^{V_c} = \sigma_0 E_0^2 / (1 - f_s)$  (see SM-V [13]):

$$\frac{\mu_{\text{hom}}}{\mu_0} = \varphi (1 - f_s) \frac{\overline{\vec{e} \cdot \vec{e}}^{V_c}}{E_0^2}. \quad (9)$$

We then define a measure of the fluctuation density in the form of the ratio of the quadratic average and the square of the linear average of the electric field by eliminating  $E_0$  in between Eqs. (3) and (9),

$$\frac{\overline{\vec{e} \cdot \vec{e}}^{V_c}}{(\vec{e} \cdot \vec{n}_z)^2} = \frac{\varphi}{(1 - f_s)} \left( \frac{\sigma_{\text{hom}}}{\sigma_0} \right)^{-2} \frac{\mu_{\text{hom}}}{\mu_0}, \quad (10)$$

where  $\varphi/(1 - f_s)$  is recognized as the CB concentration in the volumetric wiring. In Fig. 4(a), we plot the experimental fluctuation density,  $Y = \overline{\vec{e} \cdot \vec{e}}^{V_c} / (\vec{e} \cdot \vec{n}_z)^2$  [Eq. (10)] vs

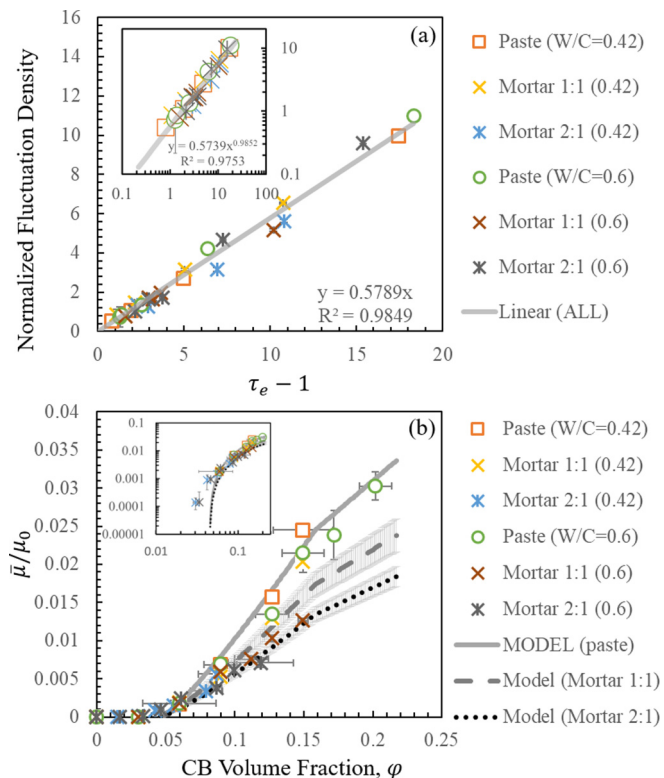


FIG. 4. Fluctuation-based assessment of Joule effect. (a) Normalized fluctuation density  $Y$  (see text) vs excess tortuosity  $X = \tau_e - 1$  [ $\tau_e = 1$  is the “perfect” (imperfection-free) conductor]. Inset: Log-log plot with a power fit  $Y = \alpha x^\beta$ , with  $\beta \approx 1$ , confirming the linear scaling  $Y \sim X$ . (b) Model performance for normalized resistive heating,  $\mu_{\text{hom}}/\mu_0 = \varphi(1 - f_s)/[2(1 + \tau_e)]$ , vs carbon-black volume fraction  $\varphi$ . Inset: model performance in a log-log scale.

$X = \tau_e - 1$ . The rationale behind this data display is that (i) tortuosity captures the deviation from a straight streamline flow of electrons through the sample, and is thus a prime candidate to capture electric-field fluctuations and related dissipation; and (ii) fluctuations should vanish for  $\tau_e = 1$ . The linear scaling of the fluctuation density with tortuosity,  $Y \sim X$ , is evidenced in Fig. 4(a). Finally, a substitution of this linear relation in Eq. (10) provides a means to highlight the competition between conductor concentration  $\varphi$  and electric tortuosity  $\tau_e$  in the development of the resistive heating capacity of the composite,

$$\frac{\mu_{\text{hom}}}{\mu_0} \sim \varphi(1 - f_s) \left( \frac{1}{\tau_e} - \frac{1}{\tau_e^2} \right) \cong \frac{\varphi(1 - f_s)}{1 + \tau_e}, \quad (11)$$

where we considered a Taylor series expansion,  $(1 + \tau_e)^{-1} = \tau_e^{-1} - \tau_e^{-2} + O(\tau_e^{-3})$ . That is, as  $\varphi$  increases, the electric tortuosity decreases [Fig. 3(a)] until it reaches a minimum,  $\tau_e(\varphi > \varphi_0) = \tau_e(\varphi_0)$ , at which the volumetric wiring saturates

the bulk, and beyond which the Joule heating is expected to linearly increase with the conductor concentration within the range of values considered in our investigation,  $\varphi < 25\%$ .

The predictive power of the resistive heating model, given by Eq. (11), is shown in Fig. 4(b). While the model slightly overestimates the percolation threshold [inset of Fig. 4(b)] which is a consequence of the tortuosity model, as a first-order model ( $R^2 = 0.9775$  above percolation threshold), it rationalizes the increase and dilution of the Joule effect with the concentration of, respectively, the conductor (carbon black) and the insulator (sand).

#### IV. CONCLUDING REMARKS

In summary, our hybrid experimental-theoretical approach provides evidence that in addition to the conductor volume concentration, (i) the electric tortuosity defines much of the electric conductivity of nCB-cement-based composites, and (ii) the resistive heating (or Joule effect) of electron conductive bulk composites is controlled by electric-field fluctuations—reminiscent of the fluctuation-dissipation theorem. This volumetric heat rate results from the dissipation of electric-field energy due to intrinsic imperfections of the conducting volumetric wiring in the conductor-insulator composite, which, in first order, is well captured by functional relations of the electric tortuosity,  $\tau_e$ . Our semiempirical fluctuation-tortuosity model predicts that rationalizing the design of electron conducting bulk composite materials will ultimately focus on settling the competition between conductor concentration and electric tortuosity, with electric tortuosity tailored by engineering the texture design. The quantitative assessment model and its future refinements open venues for harvesting new functionalities of classical commodity materials such as concrete for existing and emerging green technology applications, ranging from radiant heating to energy storage. Given the global environmental impact of the production of cement-based materials [8], the development and implementation of such novel functionalities is expected to foster the sustainable development of both the construction sector and our built infrastructure at large.

#### ACKNOWLEDGMENTS

Research carried out by the CSHub@MIT, with sponsorship provided by the Portland Cement Association and the Ready Mixed Concrete Research & Education Foundation. N.A.S. is grateful for financial support from the Natural Sciences and Engineering Research Council of Canada (NSERC) and Fonds de Recherche du Québec Nature et Technologies (FRQNT). V.D. acknowledges the financial support of his internship by the joint MIT-CNRS research unit funded through CNRS, France.

- [1] P. Xie, P. Gu, Y. Fu, and J. Beaudoin, Conductive cement-based compositions, U.S. Patent No. 5,447,564 (5 September 1995).  
 [2] D. D. L. Chung, *Multifunctional Cement-based Materials* (Marcel Dekker, New York, 2003).

- [3] G. Pye, R. Myers, M. Arnott, J. Beaudoin, and P. J. Tumidajski, Conductive concrete composition, U.S. Patent No. 6,503,318 B2 (7 January 2003).  
 [4] D. D. L. Chung, Electrically conductive cement-based materials, *Adv. Cem. Res.* **16**, 167 (2004).

- [5] S. Mingqing, M. Xinying, W. Xiaoying, H. Zuofu, and L. Zhuoqiu, Experimental studies on the indoor electrical floor heating system with carbon black mortar slabs, *Energy Build.* **40**, 1094 (2008).
- [6] J. Gomis, O. Galao, V. Gomis, E. Zornoza, and P. Garcés, Self-heating and de-icing conductive cement. Experimental study and modeling, *Constr. Build. Mater.* **75**, 442 (2015).
- [7] R. J. M. Pellenq, K. Ioannidou, N. Chanut, T. Divoux, R. Backov, and F.-J. Ulm, Electron conducting carbon-based cement, U.S. Patent No. US20190218144 (18 July 2019).
- [8] K. Van Vliet, R. Pellenq, M. J. Buehler, J. C. Grossman, H. Jennings, F. J. Ulm, and S. Yip, Set in stone? A perspective on the concrete sustainability challenge, *MRS Bull.* **37**, 395 (2012).
- [9] P. J. Tumidajskia, P. Xiea, M. Arnott, and J. J. Beaudoin, Overlay current in a conductive concrete snow melting system, *Cem. Concr. Res.* **33**, 1807 (2003).
- [10] C. Y. Tuan, Roca Spur Bridge: The implementation of an innovative de-icing technology, *J. Cold Reg. Eng.* **22**, 1 (2008).
- [11] B. Han, S. Sun, S. Ding, L. Zhang, X. Yu, and J. Ou, Review of nanocarbon-engineered multifunctional cementitious composites, *Compos. Part A Appl. Sci. Manuf.* **70**, 69 (2015).
- [12] W. Ma and D. Zhang, Multifunctional structural supercapacitor based on graphene and magnesium phosphate cement, *J. Compos. Mech.* **53**, 719 (2018).
- [13] See Supplemental Material at <http://link.aps.org/supplemental/10.1103/PhysRevMaterials.4.125401> for details are provided on material design and optimization and model derivations.
- [14] W. Zhang, A. A. Dehghani-Sani, and R. S. Blackburn, Carbon based conductive polymer composites, *J. Mater. Sci.* **42**, 3408 (2007).
- [15] S. Kirkpatrick, Percolation and conduction, *Rev. Mod. Phys.* **45**, 574 (1973).
- [16] C. C. Chen and Y. C. Chou, Electrical-Conductivity Fluctuations Near the Percolation Threshold, *Phys. Rev. Lett.* **54**, 2529 (1985).
- [17] I. Balberg, A comprehensive picture of the electrical phenomena in carbon black polymer composites, *Carbon* **40**, 139 (2002).
- [18] B. Nigro, C. Grimaldi, P. Ryser, F. Varrato, G. Foffi, and P. J. Lu, Enhanced tunneling conductivity induced by gelation of attractive colloids, *Phys. Rev. E* **87**, 062312 (2013).
- [19] J. J. Richards, J. B. Hipp, J. K. Riley, N. J. Wagner, and P. D. Butler, Clustering and percolation in suspensions of carbon black, *Langmuir* **33**, 12260 (2017).
- [20] H. H. Hassan, E. M. Abdel-Bary, M. Amin, M. K. El-Mansky, and M. E. Gouda, Thermal effects of heat-resistant rubber blends. I. Joule heating effects in carbon blackloaded NR/SBR blends, *J. Appl. Polym. Sci.* **39**, 1903 (1990).
- [21] H. H. Hassan, E. M. Abdel-Bary, M. K. El-Mamy, S. E. Gwaily, and N. M. Shash, Thermal effects of heat-resistant rubber composites. III. Effect of type and concentration of carbon black, *Mater. Chem. Phys.* **36**, 161 (1993).
- [22] Safety Data Sheet PBX-55 Carbon Black (Cabot Corp.), <https://www.cabotcorp.cn/Datasheet-PBX-55pdf.pdf>.
- [23] D. Stauffer and A. Aharony, *Introduction to Percolation Theory*, revised 2nd ed. (Taylor and Francis, London, 2010).
- [24] D. Mikuli, B. Milovanovi, and I. Gabrijel, Analysis of thermal properties of cement paste during setting and hardening, in *Non-destructive Testing of Materials and Structures*, RILEM book series, Vol. 6, edited by O. Gunes and Y. Akkaya (Springer, Dordrecht, 2013).
- [25] *Continuum Micromechanics*, CISM Courses and Lectures, Vol. 377, edited by P. Suquet (Springer, New York, 1997).
- [26] L. Dormieux, D. Kondo, and F.-J. Ulm, *Microporomechanics* (Wiley and Sons, Chichester, UK, 2006).
- [27] L. Dormieux and E. Lemarchand, An homogenization approach of advection and diffusion in cracked porous material, *J. Eng. Mech.* **127**, 1267 (2001).
- [28] B. Ghanbarian, A. G. Hunt, R. P. Ewing, and M. Sahimi, Tortuosity in porous media: A critical review, *Am. J. Soil Sci. Soc.* **77**, 1461 (2013).
- [29] H. Saomoto and J. Katagiri, Direct comparison of hydraulic tortuosity and electric tortuosity based on finite element analysis, *Theor. Appl. Mech. Lett.* **5**, 177 (2015).
- [30] A. Sur, J. L. Lebowitz, J. Marro, M. H. Kalos, and S. Kirkpatrick, Monte Carlo studies of percolation phenomena for a simple cubic lattice, *J. Stat. Phys.* **15**, 345 (1976).
- [31] A. Zaoui, Structural morphology and constitutive behaviour of micro heterogeneous materials, in *CISM Courses and Lectures*, Vol. 377, edited by P. Suquet (Springer, New York, 1997).
- [32] B. Marinho, M. Ghislandi, E. Tkalya, C. E. Koning, and G. de Witha, Electrical conductivity of compacts of graphene, multi-wall carbon nanotubes, carbon black, and graphite powder, *Powder Technol.* **221**, 351 (2012).
- [33] X. Chateau, G. Ovarlez, and K. Luu Trung, Homogenization approach to the behavior of suspensions of noncolloidal particles in yield stress fluids, *J. Rheol.* **52**, 489 (2008).
- [34] F. Nicot, N. P. Krut, and O. Millet, On Hills Lemma in continuum mechanics, *Acta Mech.* **228**, 1581 (2017).